INFLUENCE OF WELD-SEAMS ON THE FLUID-STRUCTURE-INTERACTIONS IN PIPE FLOWS

Mario Kuschewski[1], David Klören[1,2], Rudi Kulenovic[1], Eckart Laurien[1]

[1]Institute of Nuclear Technology and Energy Systems (IKE), University of Stuttgart, Germany
[2]EnBW Kernkraft GmbH, Kernkraftwerk Neckarwestheim, Neckarwestheim, Germany

Abstract. The joint research project 'Thermal Fatigue - Basics of the system-, outflow- and material-characteristics of piping under thermal fatigue" funded by the Federal Ministry of Education and Research is an ongoing German research project. The introduced part of one sub-project aims at the fluid-mechanical modelling for coupled fluid-structure-simulations. This paper presents experiments and CFD simulations of fluid dynamics close to a welding seam model. The Particle-Image-Velocimetry (PIV) method is applied to measure velocity profiles in a straight pipe and a T-junction configuration. The Near-Wall-LED-Induced-Fluorescence technique is used to investigate the mixing close to the wall. The results obtained by both methods are compared to large-eddy simulations (LES).

1 INTRODUCTION

Unsteady non-isothermal fluid flows, known for instance from power plants, cause temperature fluctuations in pipes. Crack initiation must be expected for specific components after some hundreds of hours. In general, the common problems link to plug-type transients, steady state stratification effects and the associated Low Cycle Fatigue (LCF) are acceptably understood and can be controlled by plant instrumentation systems [1]. In the past engineers faced problems regarding turbulent non-isothermal fluid mixing, for instance in piping systems with bows and T-junctions combining coolant injection line and a hot fluid line. By today external surface thermocouples can not monitor the highly transient temperature fields and therefore provide no information about the High Cycle Fatigue (HCF).

Due to missing input data regarding fast transients, mixing zones etc., the existing tools for the prediction of the HCF are not reliable for actual conditions and include broad safety margins which are considered to be too conservative. Latter causes frequent non-destructive investigations and exchange of components. The replacement of components is of special importants for nuclear installations because it is not reasonable to run a 'leak before exchange' approach.

According to recent developments in international ageing management activities, the proactive approach to avoid and minimize premature ageing is promoted. For this task knowledge about the transients and the fluid-structure-interactions (FSI) must be available in the modelling / design stage. The FSI is not yet understood and needs further investigations for advanced computational models. In this context experiments are needed for the validation of new multi-physical models which take into account the heat transfer from fluid to wall and vice versa.

2 THERMOHYDRAULICS

According to generic data provided by Électricité de France SA (EDF) weld seams are of special interest. Remaining seams in the inside of the pipes disturb the fluid flow. In the case of non-isothermal fluid mixing cracks are often observed in circumferential welds or in the smooth base material close to them. Non-isothermal mixing is not restricted to the intersections and components where the fluid flows intersect. Even for axial positions far downstream temperature fluctuations close to the wall can have amplitudes relevant for thermal fatigue especially for cases with low turbulence. The schematic drawing shown in Fig. 1 points out HCF damage observed in the neighbourhood of a T-junction [2]. Characteristic for the damage regions are networks of cracks (elephant skin type damage), groups of parallel cracks and linear defects. Additionally networks of cracks were found downstream of the T-junction. It is commonly agreed that temperature fluctuations with frequencies in the range of 2 Hz to 20 Hz are responsible for HCF [3].

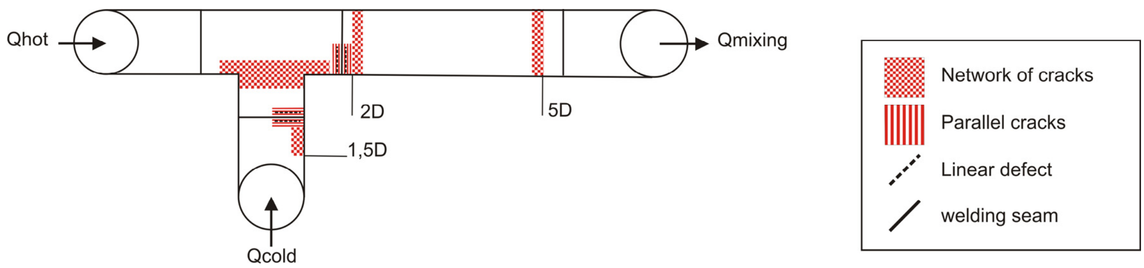

Figure 1. T-junction configuration with indicated pipe defects in the mixing zone and downstream of the intersection [2]

3 TEST RIG FOR COLD CONDITIONS

The experiments were conducted under cold conditions. The test rig comprises an open loop with two separated supply tanks and a waste water tank. For each tank an immersion pump is used to either control the mass flux for the inlets or empty the waste tank. Ball valves and inclined seat valves are installed for the fine adjustment. The inner diameters (ID) of the pipes were selected to 35.5 mm and 71 mm for the branch resp. main line. Both pipes had inlet conditioners utilising screens and rectifiers. They are connected to inlet lines with inflow lengths longer than 48 ID. For the optical access a glass tube is used. It is surrounded by an aquarium made of transparent PVC and glass elements. It is filled with water to compensate the refractive index difference of water, glass and air. A simplified schematic of the piping and instrumentation is shown in Fig. 2.

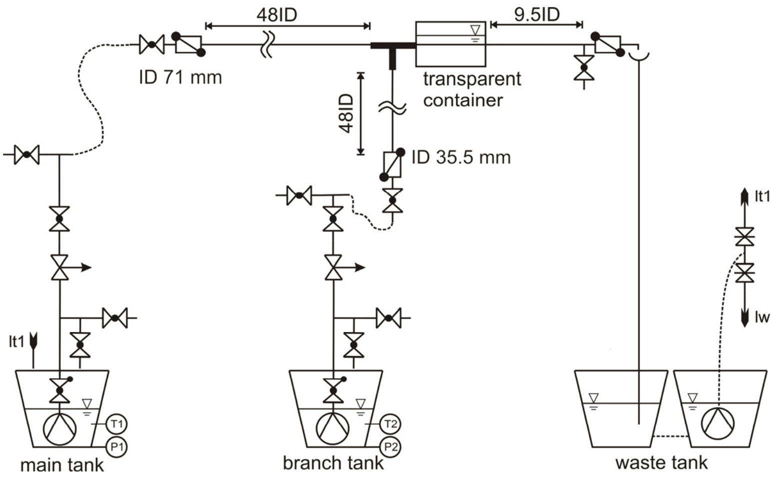

Figure 2. Test rig with T-junction and transparent container for optical access

Downstream of the transparent container two pipe elements are installed before a hose feeds the water in the waste tank. Each one has a length of 340 mm (4.7 ID of main line) so that a feedback of the out flowing fluid can be neglected. The T-junction is only installed for the investigation of T-junction mixing. For a straight pipe configuration it is removed and the inlet line is directly connected to the transparent container.

4 MEASUREMENT SETUPS

4.1 Measurement Methods

For the validation of computational fluid dynamics models it is essential to collect information regarding the boundary conditions. The mass flow rates and the corresponding mean temperatures are measured conventionally (flowmeters, thermocouples). For the determination of fluid velocity distributions the Particle-Image-Velocimetry (PIV) technique was used.

For the classical two-components planar PIV (2C-PIV) an optical access with two perpendicular windows is needed (see Fig. 3). A sheet of laser light is orientated through one window parallel to the pipe axis. A special PIV-camera is installed perpendicular to the light sheet and zooms on seeding particles in the flow illuminated within the light sheet. Comparing a time-series of images makes it possible to detect the movement of groups of particles in the time intervals between the images.

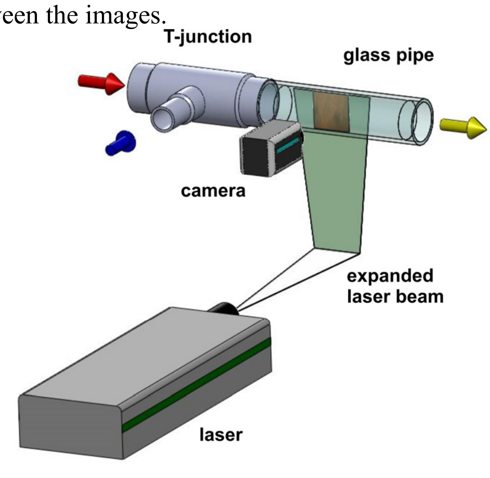

Figure 3. Particle-Image-Velocimetry setup

The time differences are known, thus the velocity of particle groups can be expressed in pixels per second. By means of a length calibration it is possible to map pixel values to real dimensions and ultimately calculate local velocity distributions i. e. the two velocity components within the measurement plane (light sheet).
Classical optical methods like the PIV technique can not be used for systems with refractive index differences >0.25*%*, this corresponds to a density difference of 1*%* in water e.g. thermally induced by a temperature difference of 30*K*. Due to this reason PIV is restricted to cases without or very small density differences and for all others it is necessary to apply new optical methods which focus on the near wall regime. The so called Near-Wall-LED-Induced-Fluorescence method utilises a measurement of instationary temperature or density fields close to the wall. It is based on the use of fluorescent dyes with temperature dependant properties. One or more dyes are solved in the fluid and a LED source excites the dye molecules close to the wall. The setup is shown in Fig. 4.

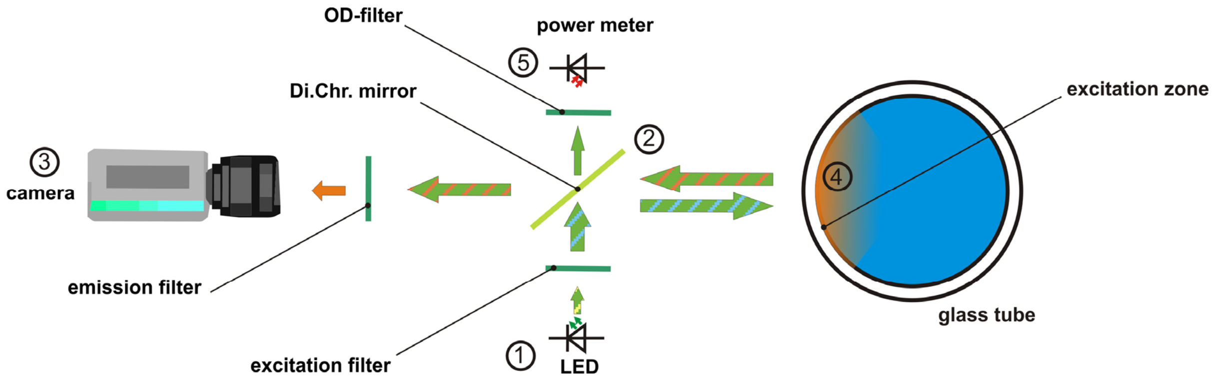

Figure 4. Near-Wall-LED-Induced-Fluorescence setup

A LED spotlight (1) emits green light cleaned up with an excitation filter. The diachronic mirror (2) deflects the light in the direction of the pipe. Its reflectivity is a function of wavelength so that a camera (3) can detect the fluorescence light which comes from the excitation zone (4) and passes the emission filter. By means of the power meter the LED power is monitored.
The position of the camera for both measurement techniques remained the same for all described measurements.

4.2 Welding Model and T-junction

The test rig consists of drawn polymer tubes, notches and gaps are reduced to a minimum to prevent any influence. The only geometrical discontinuity extending into the pipe was the welding seam model (see Fig. 5). It is a torus made from stainless steel whose outer diameter has been reduced. Less than the half of the ring remained so that the contact angle between glass and ring was smaller than 90° and therefore closer to a real weld. A slot was machined so that the torus could be used as spring and placed into the glass pipe.

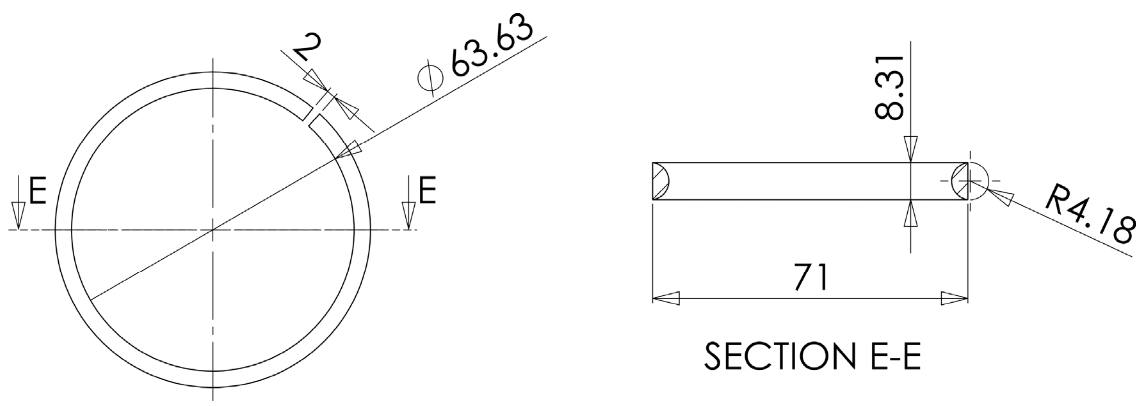

Figure 5. Drawing of the weld model

The T-junction was machined from a monolithic polyoxymethylene (POM) block. The material is especially suitable for precise prototyping and the monolith enabled a one piece construction without steps. The edge at the intersection of the flow steams is only slightly grinded. The radius of curvature is smaller than 0.2 mm.

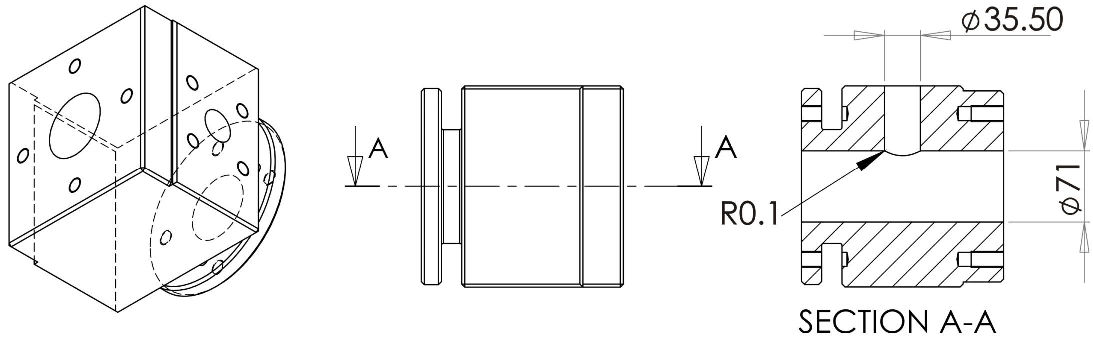

Figure 6. Drawing of the T-junction made of POM

5 PIV EXPERIMENTS

5.1 Overview

In Tab. I the chosen cases for the PIV experiments are shown. First a straight pipe was investigated and afterwards a T-junction configuration. For both geometries experiments with and without the welding seam model were conducted.

Table I. System settings and fluid parameter for the PIV experiments

Experiment no.	T_{main} [°C]	T_{branch} [°C]	Q_{main} [l/s]	Q_{branch} [l/s]	Geometry	Welding seam	PIV puls-puls-delay
1	20	-	1	---	Pipe	NO	2 ms
2	20	-	0.75	---	Pipe	NO	3 ms
3	20	-	0.5	---	Pipe	NO	3 ms
4	20	-	1	---	Pipe	YES	2 ms
5	20	-	0.75	---	Pipe	YES	3 ms
6	20	-	0.5	---	Pipe	YES	3 ms
7	20	20	0.4	0.1	T-junction	YES	3 ms
8	20	20	0.8	0.2	T-junction	YES	1.2 ms
9	20	20	0.8	0.4	T-junction	YES	0.9 ms
10	20	20	0.75	0.75	T-junction	YES	0.9 ms
11	20	20	0.4	0.1	T-junction	NO	3 ms
12	20	20	0.8	0.2	T-junction	NO	1.2 ms
13	20	20	0.8	0.4	T-junction	NO	0.9 ms
14	20	20	0.75	0.75	T-junction	NO	0.9 ms

For the straight pipe investigations the transparent container was directly connected to the inlet pipe. Latter was 2.6 times of the main pipe diameter upstream of the weld model which was fitted in the glass pipe. Looking downstream its slot was oriented at 7:30 o'clock position. The fit was tight so that the weld could not move and the gap between steel ring and glass wall was minimal. For the T-junction investigations its position remained the same yet the T-junction was installed between the inlet pipe and the transparent container.

For the straight pipe investigations the selected seeding particles IM30-K were provided by the company 3M. For the T-junction experiments HGS-10 particles from Dantec Dynamics were used. Some of the properties of the two seeding materials are collected in Tab. II:

Table II. Properties of the seeding particles

Name	Type	Mean diameter / distribution	Density
IM 30 - K	Expanded hollow glass spheres	9 μm ,17 μm ,25 μm (10%/50%/90%)	1.4 g/cm^3
HGS – 10	Expanded hollow glass spheres	10 μm	0.6 g/cm^3

The collection of the data and the post-processing were performed with the software Dynamic Studio V3.14 from Dantec Dynamics.

For the analysis of the double pictures a set of pre-processing steps were needed:

- Determining the scaling factor on the basis of a reference picture
- Calculation of the mean including all pictures
- Background subtraction of the mean picture
- Extraction of the interesting part of the pipe (region of interest: ROI)
- Adaptive Correlation
    - Final interrogation area (IA) size 64 x 32 (HxV)
    - Overlap (50%/50%)
    - Central interrogation area offset
    - Peak to peak fraction >1.3
    - Refinement steps 2
    - Number of multi passes per step (initial 2, intermediate 2, final 2)
    - Subpixel refinement
- Range Validation
- Moving Average Validation
- Vectors statistics of all vectors who passed all validation criteria

Table III. Recording parameter for the PIV experiment

Camera	FlowSense 4M
Objective	Zeiss Macro Planar T* 2/50 + 5 mm offset ring
f-stop	22
Trigger rate	7.4 Hz
Image pairs	400
Pixel pitch	7.4 um x 7,4 um
Picture size	75.776 x 75.776 mm
Number of double frames	400
Resolution	12 Bit
Laser sheet thickness	approx. 1 mm
Alignment/positioning/image size calibration	+/- 0.5 mm
Maximum displacement	9 to 14 pixels
Particle image diameter	3-4 pixels

5.2 Experimental Results for Straight Pipe

The pressure sensor signals were evaluated first. The recorded voltages correspond to pressure which are linked to water levels in the supply tanks. A 4th order polynomial is used to derive the transient water level from which the flow rate is determined.

The vectors fields provide velocity profiles from different axial positions. For the calculation of the flow rate, velocity profiles taken at the most upstream axial positions were analysed. The results of the integrations (trapezoid summation) are shown in Tab. IV.

Table IV. Flow rate measurements for Exp. 1 - Exp. 6

Experiment no.	Pressure Sensor		PIV	
	Q_{main} [l/s]	Q_{branch} [l/s]	Q Mixing section [l/s]	Valid detection rate (VDR)
1	1.00 +/- 0.10	---	1.23	~ 94 %
2	0.75 +/- 0.08	---	0.98	~ 96 %
3	0.50 +/- 0.07	---	0.66	~ 93 %
4	0.85 +/- 0.09	---	1.13	~ 93 %
5	0.71 +/- 0.07	---	0.99	~ 91 %
6	0.52 +/- 0.06	---	0.67	~ 96 %

The differences between the pressure sensor data and the PIV results were evaluated extensively. It resulted in the decision to use only the flow rates from PIV measurements which were sufficiently precise.

In Fig. 7 the mean velocity profiles for the cases with and without welding seam at the axial position x/D = 0.3 (d: main pipe inner diameter) downstream of the weld position are shown. The mean velocities are not varying as a function of the flow rate although the welding changes the shape of the profiles. They are flattened in the centre of the pipe while the gradients close to the wall are reduced.

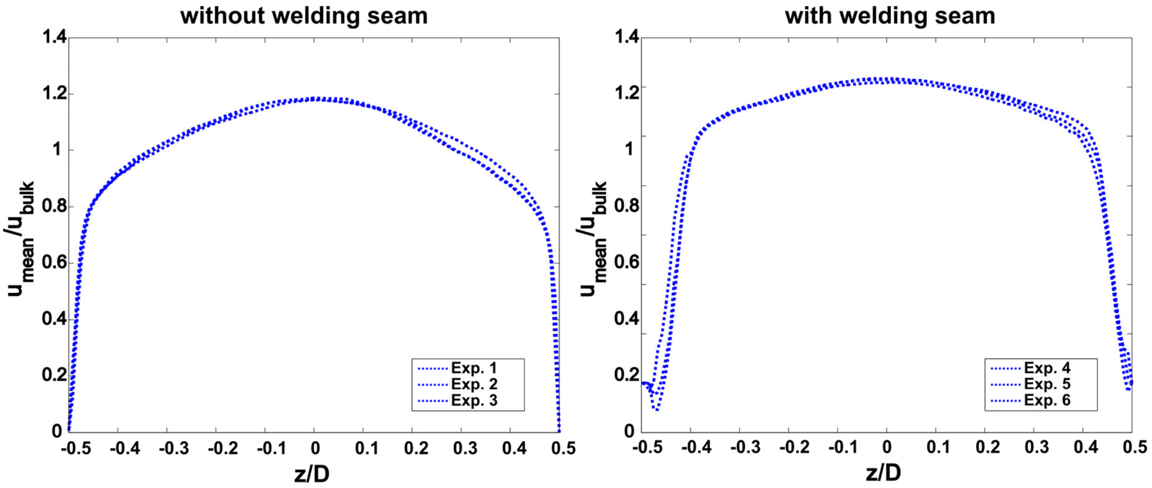

Figure 7. Mean velocity profiles x/D = 0.3 downstream of welding seam position for Exp. 1 – Exp. 6

In Fig. 8 the RMS values of the axial velocity component for the straight pipe cases with installed welding seam are shown. The fluctuations have a minimum in the middle of the pipe and increase towards the walls up to 35% of U_{bulk} (mean of the velocity profil). While the RMS values for Exp. 4 (1.13 *l/s*) and 5 (1.0 *l/s*) are nearly the same, the values for Exp. 6 (0.67 *l/s*) drop to about 27%.

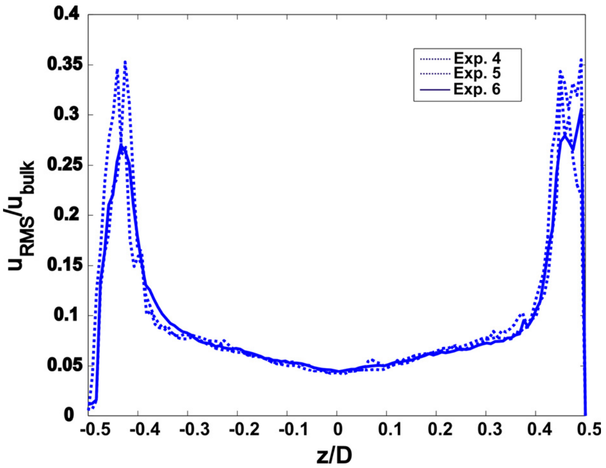

Figure 8. RMS profiles x/D = 0.3 downstream of welding seam for Exp. 4 – Exp. 6

5.3 Experimental Results for T-junction Investigations

In Tab. V the chosen settings for the PIV experiments 7 to 14 are shown. The data for the branch flow rates for Exp. 11 to 14 were not recorded. However, the PIV data shows good agreement with the previous flow settings and therefore Exp. 11 to 14 are taken into account for comparison.

Table V. System settings and fluid parameter for the test experiment

Experiment no.	Pressure Sensor		PIV	
	Q_{main} [l/s]	Q_{branch} [l/s]	Q Mixing section [l/s]	Valid detection rate (VDR)
7	0.41 +/- 0.07	0.16 +/- 0.06	0.68	~ 90 %
8	0.74 +/- 0.08	0.33 +/- 0.07	1.29	~ 92 %
9	0.72 +/- 0.07	0.51 +/- 0.07	1.43	~ 92 %
10	0.73 +/- 0.08	0.96 +/- 0.08	1.76	~ 84 %
11	0.38 +/- 0.06	*	0.70	~ 88 %
12	0.77 +/- 0.07	*	1.30	~ 89 %
13	0.73 +/- 0.07	*	1.42	~ 89 %
14	0.73 +/- 0.08	*	1.76	~ 82 %
				* data not available

The noticeable lower valid detection rates of T-junction experiments are not related to the change of seeding particles. The concentration and the particle picture size remained the same yet the in-plane components increased.

The resulting vector maps of PIV experiment no. 7 was analysed and the streamlines calculated. The result is shown in Fig. 9. The flow enters the measurement region from left and passes the welding seam.

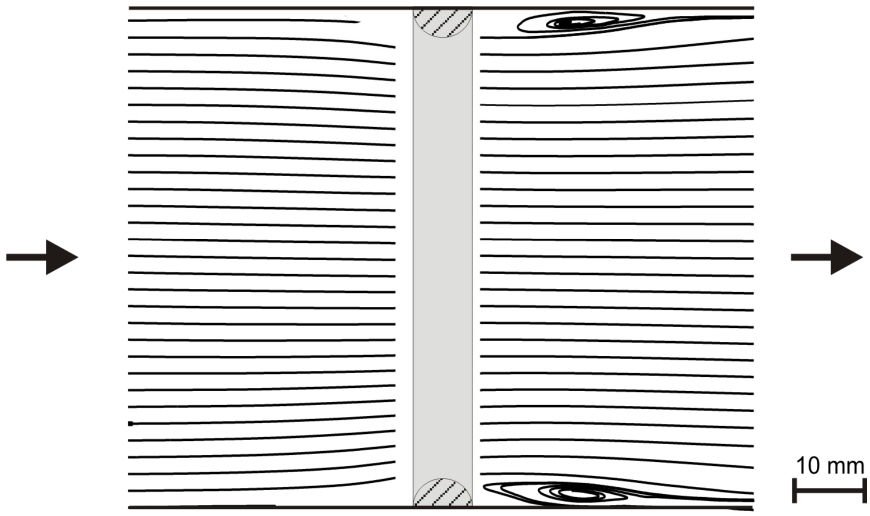

Figure 9. Streamlines for T-junction Experiment no. 7

Two recirculation zones can be identified downstream of the welding seam. They extent to about 3 diameter downstream of the weld which corresponds to x/D = 0.23. One can also see the compression of streamlines close to the weld which is usually the case for a flow contraction. The injection of a larger amount of light seeding particles brought some more insight. It accumulated upstream of the weld in a small recirculation zone no longer than a third of the welding seam length.
The mean axial velocities for Exp. 7 – 14 are shown in Fig. 10. The profile characteristics are different to the

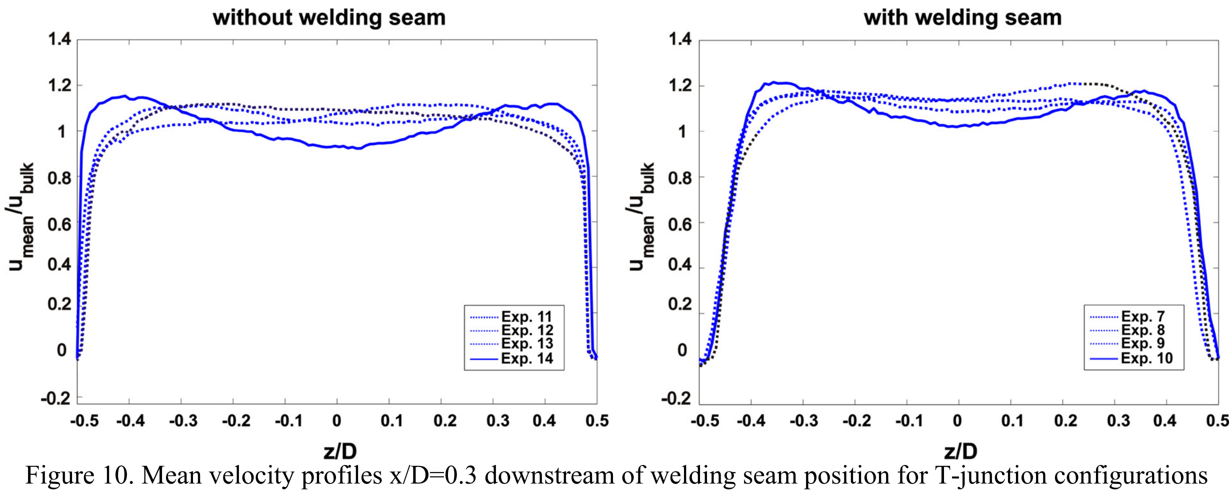

Figure 10. Mean velocity profiles x/D=0.3 downstream of welding seam position for T-junction configurations

straight pipe investigations. Even without welding model installed the profiles are flattened and shifted to one side. For all cases with welding seam installed the profiles are compressed and flattened with normalised values between 1.1 and 1.2 over 70% of the pipe diameter. The gradients near the walls are reduced compared to the straight pipe case and the standard T-junction configuration without weld. For low flow rates the profiles are a little shifted to one pipe wall while for Exp. 14 and 10 there is an M-shape profile. Latter is comparable to wake profiles and is caused by the dominant branch flow entering the main line.
The RMS-distributions for the T-junction investigations are presented in Fig. 11. They have relatively flat profile in the middle of the pipe and steep edges close to the wall. As seen before the gradients are smaller for the cases with welding seam. Without welding seam the RMS –values slightly increase with the flow rate. This tendency is not observe in the other case yet the highest flow rate has the most dominant fluctuations.
The effect of the decreased valid detection rate for Exp. 10 and 14 is an increase of the distortion superimposing the mean RMS-profile.

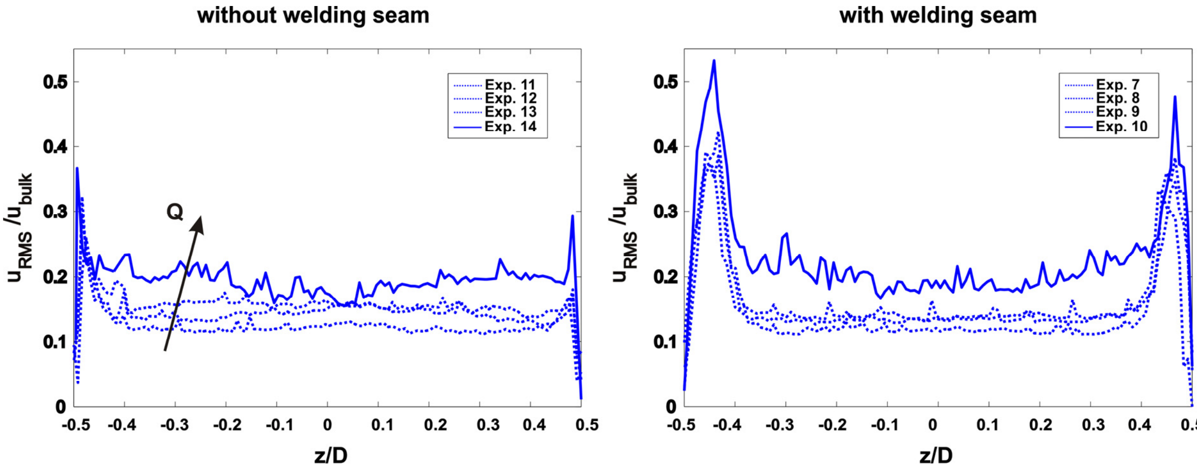

Figure 11. RMS velocity profiles x/D=0.3 downstream of welding seam position for T-junction configurations

6 NEAR WALL EXPERIMENT

6.1 Overview

In addition to the PIV technique the Near-Wall-LED-Induced-Fluorescence method was applied. The test rig configuration was the same as for the PIV T-junction experiments. The supply tank for the branch line was seeded with sugar to increase the density (simulation of FSI). For this purpose 36.35 kg sucrose was soluted in 219.6 kg tap water. The resulting density difference between the two inlet lines is equivalent to a density difference for a non-isothermal mixing of water with 20 °C and 120 °C, [4 - 8].

The welding seam was installed in the mixing zone of the T-junction x/D = 4 downstream of the intersection. Here the camera objective (60 mm AF Micro-Nikkor) was focused on the nearest inner pipe wall with f-stop 11 which offered a good illumination of the CCD-chip and low optical distortions. The Hamatsu 0804C camera was running with 2x2 binning which increased the sensitivity and the recording rate of the system to 15 frames per second. The resulting size of the observation region was 638 pixels x 504 pixels which correspond to 54.59 mm x 43.13 mm. The pictures were recorded with low gain setting and 12 bits grey levels.

In Tab. VI the settings for the FSI experiment are shown. The flow rate is based on the pressure sensor signals and is corrected for the density differences. It should be noted that the PIV result indicated an underestimated flow rate by the pressure of about 10-25 %.

Table VI. System settings and fluid parameter for the FSI experiment

	Temperature [°C]	Flow rate [l/s] from pressure sensor	Density [kg/m³]	Viscosity [mPa s]	Reynolds Nu.
main line (ID 71 mm)	20	0.182 +/- 0.09	998.21	1.0016	3253
branch line (ID 35.5 mm)	20	0.0686 +/- 0.06	1056	1.5299	1605
Combined line	20	Sum: 0.247	1013	1.077	4165

The sugar solved in the water of the branch line increases the density and the viscosity. The density fractions of sugar water mixing and hot water mixing are the same if $T_{cold} = 20\,°C$ and $T_{hot} = 120\,°C$.

$$\frac{\rho_{sugarwater(brix=14.2)}}{\rho_{water\,20°C,std.pressure}} = \frac{1056}{998.21} \approx 1.05789 \approx \frac{\rho_{water\,20°C,75bar}}{\rho_{water\,120°C,75bar}} = \frac{1001.6}{946.72} \approx 1.05797$$

The viscosity fractions are not the same for these two cases.

$$\frac{\eta_{sugarwater(brix=14.2)}}{\eta_{water\,20°C,std.pressure}} = \frac{1.5299}{1.0016} \approx 1.527 < \frac{\eta_{water\,20°C,75bar}}{\eta_{water\,120°C,75bar}} = \frac{0.99862}{0.23397} \approx 4.225$$

The fluorescent dye concentrations were selected so that the green excitation light penetrates 1 mm into the fluid.

6.2 Experimental Results

The recording of the pictures were started 10 seconds after activation of the pumps. Within 20 seconds 300 pictures were recorded. For the duration of the measurement the LED power varies +/-0.065% which did not have any effect on the measurement.
Some steps are needed for the analysis of the data:

- Dark images must be taken to correct for dark current offset
- The special fluorescence intensity distribution must be recorded as function of the excitation intensity
- Lookup of the excitation intensity for the specific records
- Calculation of the normalisation matrix:
  picture_no_offset = picture(:,:) - black_value;
  norm_matrix = 1./ picture_no_offset./max(max(picture_no_offset));
- Each picture is normalised with the normalisation matrix
- The grey values of the pictures are transformed to density values (directly proportional)
- On the basis of the standard tables provided by the International Association for the Properties of Water and Steam (IAPWS) the density values are transformed to associated temperatures

The resulting measurement error for the associated temperatures is dependent on the measured temperature itself. For the smallest associated temperatures the temperature failure for an 'isotherm' condition (just fluid from the side branch) was within +/- 2 K. For the maximum associated temperature (just fluid from the main branch) the error was within +/-12 K for single pixel analysis.

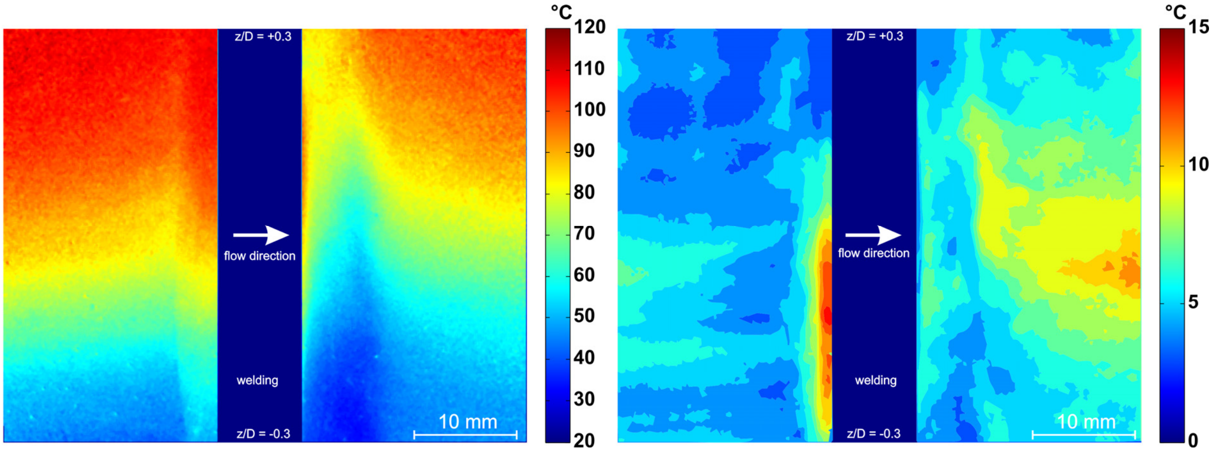

Figure 12. Stratified flow from left to right; Mean temperature field (left); standard deviation of temperature field (right)

The mean associated temperature distribution is shown in Fig. 12, left. The flow enters from left and passes the welding seam. Latter introduces two recirculation zones. One recirculation zone is situated downstream of the weld with one weld diameter in length. The other recirculation zone is upstream of the weld with a length of about 1/3 of the weld diameter. The recirculation zone downstream leads dense fluid upward while upstream the opposite is the case introducing RMS-values up to 14K (equals 14% of the temperature difference) in a zone close to and parallel to the welding seam. A similar effect cannot be seen in the second recirculation zone yet behind it.
The following definition is used to compute normalized temperatures:

$$T^* = \frac{(T - T_{cold})}{(T_{hot} - T_{cold})} \tag{1}$$

Furthermore a formulation is used for the rms-values:

$$T_{RMS} = \sqrt{\overline{((T - T_{mean})^2)}} \qquad T^*_{RMS} = \frac{T_{RMS}}{\Delta T} = \frac{T_{RMS}}{T_{hot} - T_{cold}} \tag{2}$$

The time series for the normalized temperatures was computed for three spots. One placed in the center of the highest RMS-spot and two regions were placed on the x/D=0.33 upstream and downstream of the weld on axes level. For each of these regions 5x8 pixel were selected. This corresponds to (0.428 mm x 0.68 mm. The mean temperatures for these zones were calculated and plotted over time in the diagram of Fig. 13 on the left side.

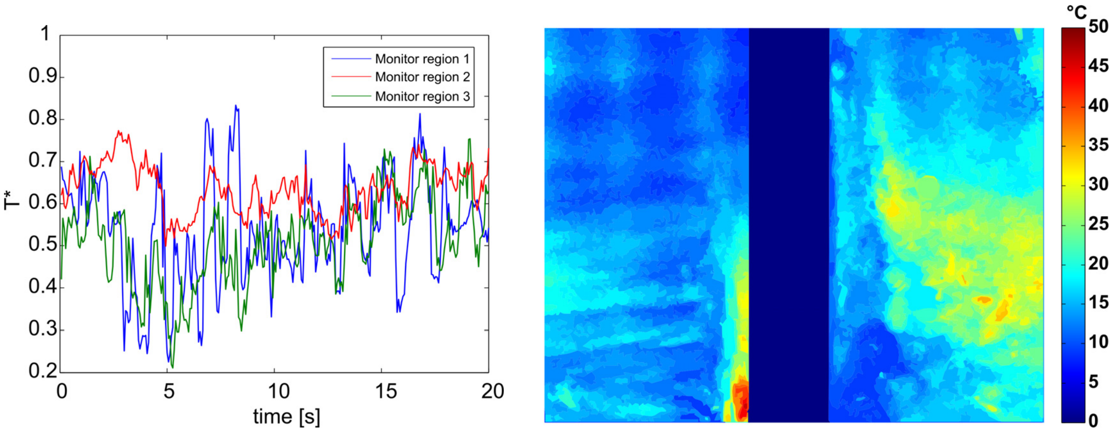

Figure 13. Temperature time series for 3 monitored regions (left); maximum deviation from local mean temperature field (right)

On the right hand side of Fig. 13 the maximum deviations from the local mean temperature (Fig. 12, left) is shown. By comparing it with the RMS-value distribution (Fig. 12, right) one can see that the spots with maximum RMS-values do not correspond directly to the regions with maximum deviation from local mean.

7 NUMERICAL STUDY

Turbulent flow induced by a welding seam and turbulent (thermal) mixing flow in a T-junction involves stagnation points, detachment and reattachment. It is therefore necessary to choose a CFD Method which performs reasonably well for these anisotropic flow phenomena. The choice of a turbulence model as well as the numerical methods is crucial to the solution quality of computational fluid dynamics (CFD). Therefore, based on the experience with simulation of T-junction flow [9], the results obtained by large-eddy simulation (LES) for both the isothermal as well as for the thermally mixing cases are investigated in this work.

7.1 Large-Eddy Simulation (LES)

LES solves the energy containing large scale turbulence without turbulence modelling, whereas turbulent structures smaller than the filter length Δ (usually coupled to the cell size in a simple manner) are modelled by subgrid scale (SGS) models in order to obtain the correct dissipation of turbulent kinetic energy. Assuming that turbulence becomes increasingly more isotropic towards the dissipation scales, simple algebraic SGS models based on the mixing length hypothesis, such as the Smagorinsky model are widely used. In this work small scale turbulence is modelled by the dynamic Smagorinsky SGS model [10]. As significant parts of the turbulent dynamics are resolved without modelling, LES has to be three dimensional and transient on a high quality mesh and is therefore computationally expensive.

7.2 Numerical methods

In the commercial finite volume solver ANSYS FLUENT the “Pressure-Implicit with Splitting of Operators” (PISO) scheme is chosen for the velocity-pressure coupling. For the spatial discretization the 2nd schemes are applied for the convection (central differencing scheme) and the pressure term. The water properties are constant values for 0.1MPa and 20°C for the isothermal cases. In case of the thermal mixing flow simulations the QUICK scheme is utilised for the energy term. The water properties are then polynomial functions of the temperature at a pressure of 7.5MPa [6]. For all cases only adiabatic wall conditions are considered. The time step is set to 1.5 ms and the physical time period exceeds at least 10s.

7.3 Meshing

The computational grid has been designed according to the guidelines of Fröhlich [11] (see Tab. VII) given in the cell size requirements for the wall adjacent control volume. The dimensionless length, height and width of the first cell from the wall surface are denoted as Δx+, Δy+ and Δz+ respectively. The superscript “+” indicates a dimensionless entity according to

$$\Delta y^{+} = \Delta y \cdot u_{\tau} / \nu \qquad (3)$$

with friction velocity u_τ and kinematic viscosity ν. Therefore, wall resolved LES is performed i.e. with sufficient resolution down to the viscous sublayer of the boundary layer for most of the computational domain.

Table VII. Guidelines for wall resolved LES by [11]

$\Delta x^+ = 50$	$\Delta y^+ = 2$	$\Delta z^+ = 15$

8 NUMERICAL TEST CASES

The numerical test cases in Tab. VIII are based on the experiments introduced above. The variation of the test cases affect the geometry (pipe and T-junction, with or without welding seam), the volume flow rate Q_1 and Q_2 and the inlet temperature T_1 and T_2 for the main pipe and the branch pipe respectively. Test case 6 is obtained by a previously performed simulation [9] using a slightly coarser grid ($2 < \Delta y+ < 20$) and the PISO based Non-Iterative Time Advancement (NITA) scheme in ANSYS FLUENT. The welding seam has the same geometry for all test cases.

Table VIII. Numerical test cases

Simulation no.	T_1 [C]	T_2 [°C]	Q_1 [l/s]	Q_2 [l/s]	Geometry	Welding seam
1	20	-	0.4	-	Pipe	Yes
2	20	-	0.8	-	Pipe	Yes
3	20	20	0.4	0.1	T-junction	Yes
4	20	20	0.8	0.4	T-junction	Yes
5	120	20	0.4	0.1	T-junction	Yes
6	120	20	0.4	0.1	T-junction	No

8.1 Pipe flow

The mean and RMS velocity profiles, normalized with the inner pipe diameter D and the bulk velocity are shown in Fig. 14 for the numerical setups Sim.1 and Sim.2 and compared against experimental data. The mean velocity profiles show similarity in terms of different volumetric flow rates at the position x/D = 0.3. This behaviour can be observed for both the numerical and the experimental results. The mean profile of experimental data appear to be slightly offset toward positive z direction.

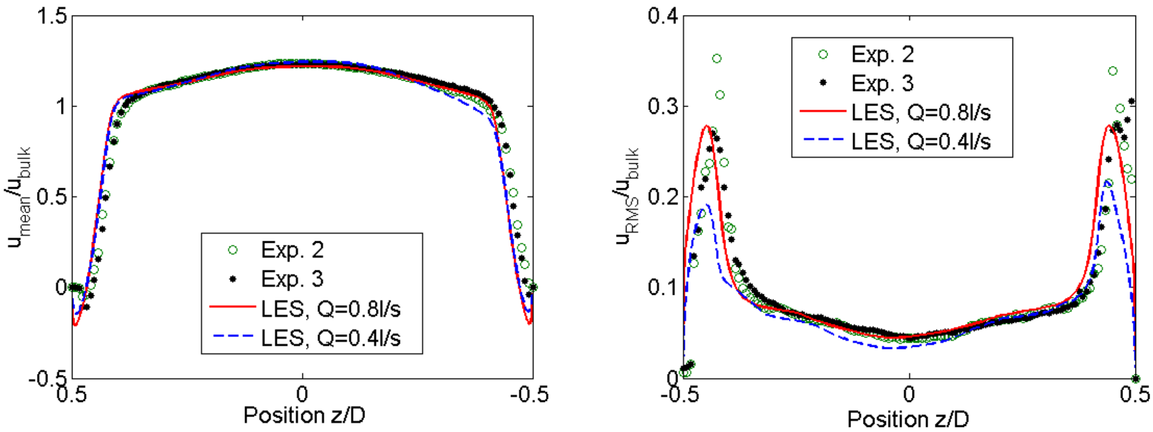

Figure 14. Mean (left) and RMS (right) of u_{mean} at x/D = 0.3 downstream of the welding seam (pipe) for simulations 1, 2 and experiments 2, 3

While the core flow profiles overlap very well, the recirculation of flow is overestimated in the simulation. Furthermore, the near wall magnitude of the velocity RMS for flows with similar flow rate is larger for the experimental data. This corresponds to the slightly steeper velocity gradients in the mean velocity profile.

The reattachment length for the separated flow depends on the mass flow rates, shown in Fig. 15 indicated by the wall shear stress transition from negative to positive values. For Q = 0.8 l/s the reattachment of the flow occurs at x/D ≈4.5, while for Q = 0.4 l/s is further downstream at x/D ≈ 0.5. As in the experiments, a higher volume flow rate corresponds to a smaller reattachment length.

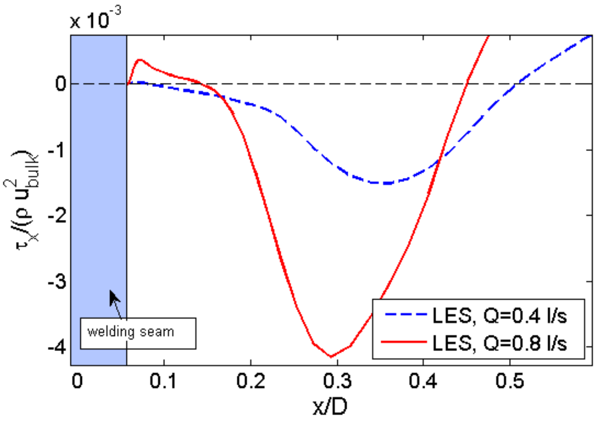

Figure 15. Normalized mean wall shear stress downstream of the welding seam (center of welding seam at x/D=0)

8.2 T-junction flow, isothermal

Fig. 16 shows the mean velocity profile (left) of experiment no. 7 and simulations no. 3 and no. 4. The mean velocity profiles show a characteristic M-shape in all cases due to the injection from the branch pipe. In contrast to the numerical results, a clear recirculating flow cannot be identified in the experimental data. Both simulations display a very strong similarity of their velocity profiles. The peaks of RMS values (Fig. 16, right) are again underestimated x/D = 0.3 downstream of the welding seam. The underestimation can be as high as 25%. However, the flat profile of the RMS values of the core flow as well the location of the RMS peaks are well reproduced. The overall similarity of the simulated profiles is nevertheless good despite the difference in absolute flow rate and the flow rate ratio of the two simulations.

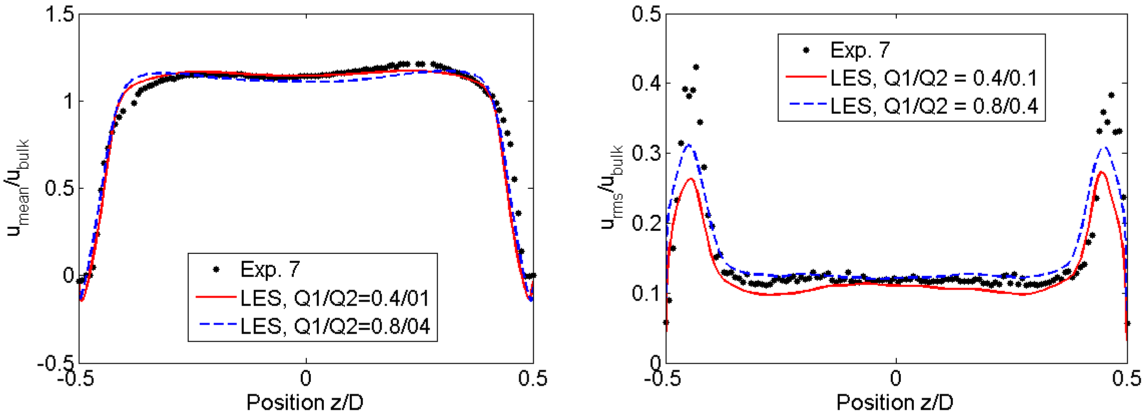

Figure 16. Mean (left) and RMS values (right) of u at x/D = 3 for the T-junction flow for simulation 3, 4 and experiment 8

8.3 T-junction flow with thermal mixing

The simulation no. 5 and no. 6 for the T-junction flow with thermal mixing including thermal stratification layer temperature profiles are shown, in Fig. 17 and Figure 18 (horizontal profiles at the position x/D = 3.9 and 4.1 with the welding seam being located at x/D = 4.0).

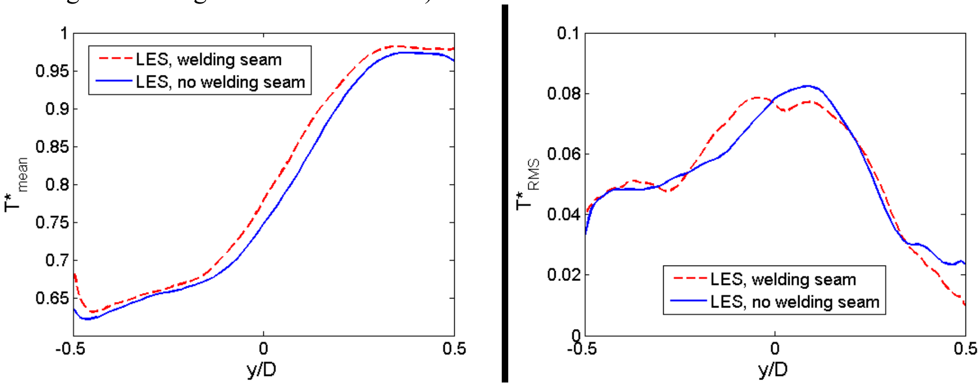

Figure 17. Mean (left) and RMS (right) of temperature at x/D = 3.9. Red - simulation with welding seam; Blue - without the welding seam [9]

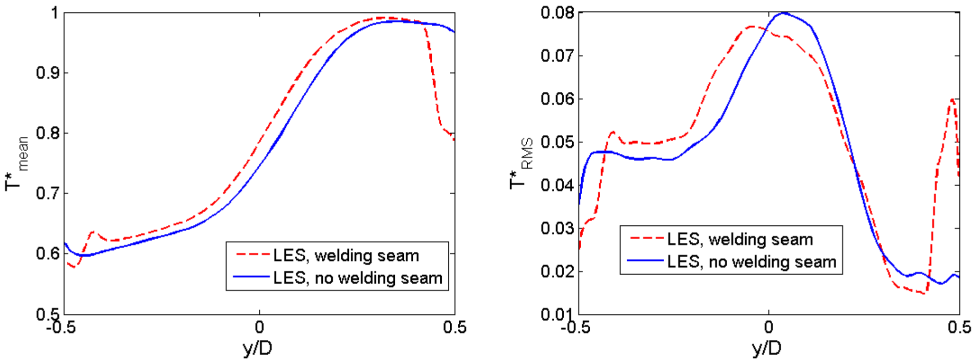

Figure 18. Mean (left) and RMS (right) values of temperature at x/D = 4.1 for the thermal mixing test case

When comparing the Simulation no. 5 and no. 6 the mean and the RMS distribution show a significant change at y/D = 0.5 (inner pipe wall). The temperature RMS is increased locally by a factor of two whereas the mean temperature has fallen nearly by 20% (Figure 18, right). Hence, the mean location of the thermal mixing layer (similar to the stratification layer) has been shifted upwards. With enhanced turbulent mixing induced by the welding seam cold water penetrates into the hot layer and causes high temperature fluctuation in the near wall region. On the opposing side at y/D = -0.5, however, the temperature fluctuation is reduced as an effect of increased mixing.

9 CONCLUSION

The influence of a welding seam on the flow field in a straight pipe and downstream of a T-junction has been investigated at a new experimental setup at the IKE. Experimental data have been measured by PIV and a new developed measurement technique using LED induced fluorescence. Numerical simulations have been carried out to investigate the performance of large-eddy simulation for this type of problems.
Isothermal experiments were conducted with varying volumetric flow rates in both the pipe and the T-junction. The normalized mean and RMS velocity profiles show a high degree of similarity for all investigated volumetric flow rates except for those T-junction configurations that had flow rate ratio (Q_{main}/Q_{branch}) close to unity or smaller.
This observation is true either with the welding seam included or not implemented in the experimental setup.
A significant influence of the welding seam on the turbulent flow field has been shown. When the welding seam is present a recirculation flow is established with a reattachment length decreasing with increasing volumetric flow rates. Therefore, the slope of the near wall mean velocity is reduced compared to experiments without the welding seam until the pipe flow has recovered further downstream. The welding seam induces shear flow which in turn creates larger RMS values of the velocity and increases the turbulent mixing.

The near wall mean and RMS of the associated temperature field upstream and downstream of the welding seam were measured by the Near Wall LED-induced Fluorescence technique. It has been observed that a recirculation zone downstream of the welding leads dense fluid upward while upstream the opposite is the case. Latter caused increased temperature RMS values parallel to the welding which resembles the crack lines of pipes subjected to high cycle fatigue due to thermal striping.
Both experiment and simulation show behaviour of similarity towards a limited variation of the mass flow rates. The influence of the welding seam on the thermal mixing is significant. The shear flow induced by the welding seam lead to increased mixing. Locally, temperature fluctuation can therefore differ strongly from the seamless condition. At the near-wall region downstream of the T-junction the welding seam is capable to give rise to temperature fluctuations as much as the T-junction induced shear flow.

10 EXPERIMENTAL SETUP FOR FUTURE INVESTIGATIONS

For future investigations a new large scale test facility is built at the University Stuttgart. A T-junction made of austenitic steel complying the German nuclear standards connects an ID 71.8 mm hot main line and a 38.9 mm branch line. The system is operating at 75 bar, and working fluid water in the branch line is 20 °C resp. in the main line at maximum temperature 280 °C. Thermocouples utilise temperature measurements near the inner pipe wall while optical modules installed in the flow path provide an optical access to the fluid. It is planned to apply PIV and the Near-Wall-Fluorescence method besides thermocouples, high temperature strain gauges and other sensors. A simplified piping and instrumentation diagram is displayed in Fig. 19.

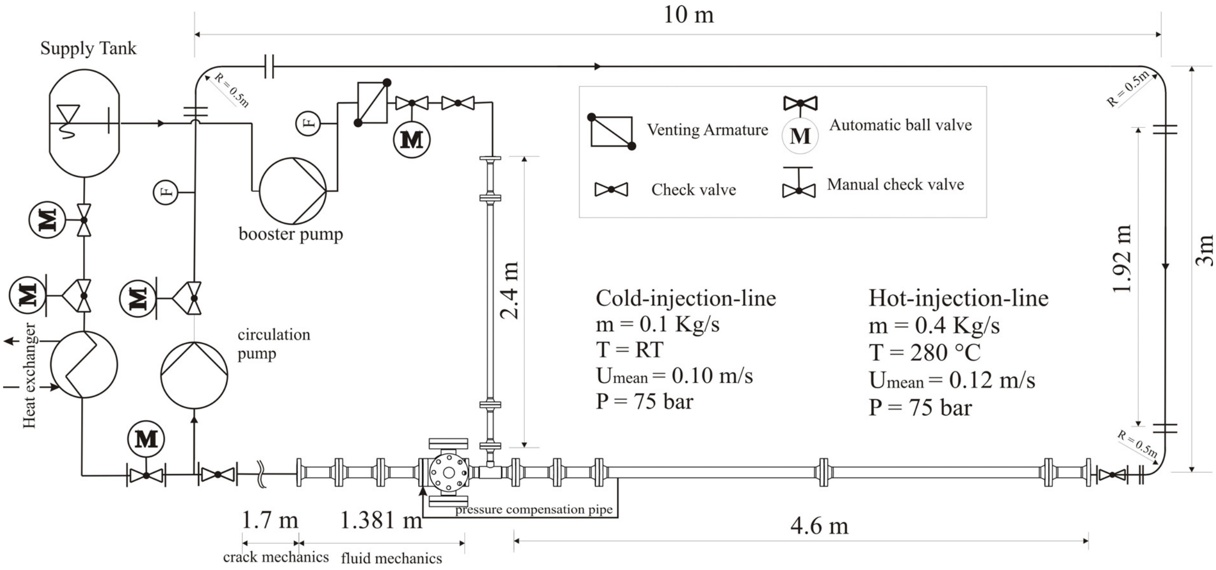

Figure 19. Fluid structure interaction setup at the University Stuttgart

11 ACKNOWLEDGEMENT

This work is carried out in the frame of a current research project funded by the German Federal Ministry of Education and Research, project number 02NUK009B. It is also supported by EnBW Kernkraft GmbH, Kernkraftwerk Neckarwestheim, Neckarwestheim, Germany.

12 REFERENCES

1- P. Hofstötter, S. Dittmar, K. Maile, K. J. Metzner, In-Service monitoring of piping and vessels in nuclear power plants: report on BMU Study SR 2218, *Nuclear Engineering and Design*, Vol. 193, 1999, pp. 233-241.

2- S. Chapuliot, Thermal fatigue in mixing areas, Overview of the industrial problem, lecture, NEA Headquarters, AREVA, 2009.

3- S. Chapuliot, Thermal fatigue in mixing areas, Keynote lecture of the Kick-Off meeting for the OECD/NEA CFD Benchmark Task, Areva, OECD/NEA, Issy-les-Moulineaux, France, 2009 May 20.

4- H. Schiweck, P. W. van der Poel, T. Schwartz, Zuckertechnologie: Rüben- und Rohrzuckergewinnung, Bartens, Germany, 2000.

5- Release on the IAPWS Formulation 1995 for the Thermodynamic Properties of Ordinary Water Substance for General and Scientific Use, 1996.

6- W. Wagner and A. Pruß, The IAPWS Formulation 1995 for the Thermodynamic Properties of Ordinary Water Substance for General and Scientific Use, *J. Phys. Chem. Ref. Data*, 31, 387, 2002.

7- A.H. Harvey, J.S. Gallagher, and J.M.H. Levelt Sengers, Revised Formulation for the Refractive Index of Water and Steam as a Function of Wavelength, Temperature and Density, *J. Phys. Chem. Ref. Data*, 27, 761, 1998.

8- Walker, D.A., 1985: A fluorescence technique for measurement of concentration in mixing liquids, *J. Phys. E:Sci. Instrum.*, Nr. 20, S. 22-24.

9- D. Kloeren, E. Laurien, Large-Eddy Simulation of Thermal Mixing in a T-junction with Conjugate Heat Transfer, NURETH 14, Toronto, Canada, Sep. 26-30, 2006.

10- M. Germano, U. Piomelli, P. Moin and W.H. Cabot, A dynamic subgrid-scale viscosity model, *Phys. Fluid*, A3, 1991, pp. 1760-1765.

11- J. Fröhlich, Large Eddy Simulation turbulenter Strömungen, Teubner-Verlag, 2006.